JOURNAL OF CATALYSIS 146, 237–248 (1994)

Estimates of Rate Coefficients for Elementary Processes Occurring during Fischer–Tropsch Synthesis over Ru/TiO_2

Takashi Komaya[1] and Alexis T. Bell

Chemical Sciences Division, Lawrence Berkeley Laboratory, and Department of Chemical Engineering, University of California, Berkeley, California 94720-9989

Received July 7, 1993; revised October 13, 1993

The dynamics of elementary processes involved in Fischer–Tropsch synthesis of hydrocarbons over Ru/TiO_2 have been determined from the analysis of data from both steady-state and transient-response experiments. Both types of experiments were carried out with different feed catalyst bed residence times to assess the effects of olefin readsorption on the dynamics of chain initiation, propagation, and termination. Strong evidence was found for the rapid reentry of ethylene into the chain growth process. The reentry of C_{3+} olefins, though, is negligible for the conditions studied. The holdup of hydrocarbons in a weakly physisorbed state was found to be significant for C_{6+} products and must be accounted for in the simulation of transient-response experiments. When the effects of ethylene readsorption and C_{6+} holdup are properly taken into account, the rate coefficients for chain initiation, propagation, and termination, determined from simulations of the transient-response experiments, are independent of carbon number and catalyst-bed residence time. Rate coefficients for the readsorption of ethylene, the depolymerization of adsorbed ethyl groups, and the dehydrogenation of methyl to methylene groups were also determined from simulations of the transient-response experiments.

INTRODUCTION

Linear olefins and paraffins are the primary products formed during Fischer–Tropsch synthesis (FTS) over Ru catalysts. Mechanistic studies (1–9) indicate that the initial step in the formation of these products is the dissociation of adsorbed CO. Hydrogenation of the nascent carbon results in the formation of CH_2 and CH_3 species that can serve as monomer and chain initiator, respectively, for the growth of hydrocarbon chains. Chain propagation occurs by the addition of CH_2 species to adsorbed alkyl groups. Linear α olefins are formed via β elimination of hydrogen from the alkyl species and normal paraffins are formed by α addition of hydrogen to alkyl species. Isotopic tracer studies have revealed that olefins, and in particular ethylene, can readsorb resulting in the formation of alkyl species some of which depolymerize to form CH_2 species (2, 10–19). The former process leads to the initiation of new chains, whereas the latter provides monomer units for additional chain growth. Readsorbed olefins can also undergo hydrogenation to form paraffins, but recent work shows that this process is strongly inhibited by CO and H_2O (18, 19).

Transient response isotopic tracer experiments have been used recently to determine the rate coefficients for chain initiation, propagation and termination (17, 20–24). Interpretation of these experiments was carried out, however, without accounting for the effects of olefin readsorption. Recent studies (17) suggest that the neglect of olefin readsorption, and in particular that of ethylene, may not be justified. For example, when ^{12}C-labeled ethylene is added to synthesis gas containing ^{13}C-labeled CO such that 24% of the carbon fed to the reactor is C_2H_4 and the balance is CO, 100% of the C_{3-8} hydrocarbon products are initiated by adsorbed C_2H_4 and 45% of the carbon atoms added by chain growth derive from C_2H_4. This paper reports the results of isotopic tracer studies aimed at establishing the effects of olefin readsorption on the dynamics of chain initiation, propagation, and termination. Also examined are the effects of the holdup of physisorbed hydrocarbons on the interpretation of transient response, isotopic tracer experiments.

EXPERIMENTAL

Catalyst Preparation and Characterization

A 1.4% Ru/TiO_2 catalyst was prepared by impregnation of TiO_2 (Degussa P-25) with an excess solution of Ru $(NO)(NO_3)_3$ (Johnson–Matthey) followed by filtration and a water wash. The impregnated support was dried in air at 383 K overnight, and then sieved to 30–60 mesh. The dried catalyst was reduced at 543 K in a flow of H_2 to minimize encapsulation of the Ru crystallites by TiO_2.

[1] Permanent address: Production Technology and Engineering Center, Mitsubishi Kasei Corporation, Kurosaki, Yahata-nishi-ku, Kitakyushu-shi, Fukuoka 806, Japan.

0021-9517/94 $6.00

The weight loading of Ru was determined by X-ray fluorescence. The chloride and sodium contents after reduction were below the detection limit (<0.02%) and 0.04%, respectively. The dispersion of Ru was determined by H_2 chemisorption to be 43.2%. The BET surface area and the average pore size, determined from a N_2 isotherm at 77 K, were 52 m^2/g and 20 nm respectively.

Apparatus

All reactions were carried out in a low dead volume quartz microreactor supplied with D_2, ^{12}CO, ^{13}CO, and He from a gas manifold (24). UHP H_2 (Matheson Gas) or D_2 (Union Carbide) was further purified by passage through a Deoxo unit (Engelhard Industries) and water was removed by a molecular sieve 13X trap. UHP CO (99.999% pure, Matheson Gas) was passed through a glass bead trap maintained at 573 K to remove iron carbonyls, an Ascarite trap to remove CO_2, and a molecular sieve trap to remove water. UHP He was passed through a molecular sieve trap to remove water. ^{13}CO (Isotec Inc, 99% ^{13}C) was used as supplied.

Product Analysis

The steady-state distribution of reaction products was determined by gas chromatography and the temporal variation in the distribution of ^{12}C and ^{13}C in each product was determined by isotopic-ratio gas chromatography/mass spectroscopy (13, 24–26). A 10-port GC sampling valve (Valco E410UWP) and a multiposition 16-sample-loop valve (Valco E6ST16T) were used to acquire and store samples. Both valves are housed in valve ovens and can be actuated electrically. Flow lines downstream of the reactor, the valve ovens, lines to the GC inlet, and lines from the GC outlet to a capillary combuster inlet were all maintained at 423 K, to minimize product condensation.

Product separation is performed by a fused silica capillary column (0.25 mm i.d. × 50 m) coated with a 1-μm film of SE-54. Products heavier than C_{14} hydrocarbons are not detected. The column effluent is split into two streams using a glass-lined capillary union (SGE); one line (0.15 mm i.d.) is sent to a FID detector for quantification, while the other transfer line (0.20 mm i.d.) is routed to a capillary combuster (13, 24). This latter stream is mixed with O_2 and combusted in CO_2 in a 2-m-long capillary (0.2 mm i.d.) containing Pt wire (0.13 mm o.d.) maintained at 873 K.

The effluent from the capillary combuster is leaked into a vacuum chamber containing the probe of a UTI 100C quadruple mass spectrometer. Complete combustion of all hydrocarbon products except methane was confirmed by the absence of peaks at masses corresponding to fragments derived from the hydrocarbons. The masses monitored by the mass spectrometer were amu 4 (He), amu 44 ($^{12}CO_2$), and amu 45 ($^{13}CO_2$). The distribution of ^{12}C and ^{13}C in C_{2+} hydrocarbons was obtained from the relative signal intensities at amu 44 and amu 45. The optimization for the temporal resolution of these products recorded by the mass spectrometer was performed by adjusting the flow rates of the two products streams and the O_2-flow for combuster by changing the length and diameter of the capillary transfer line. The resolution of C_2–C_9 hydrocarbons recorded by the mass spectrometer was comparable to that recorded by the FID.

Procedure

Experiments were carried out typically with 0.6 g of catalyst at the following conditions: T = 523 K; $CO/D_2/He$ = 1/3/6; total gas flow rate = 50 to 200 cm^3/min. For each set of conditions, the reaction was allowed to proceed in a mixture of ^{12}CO, D_2, and He for 20 min, to avoid the rapid initial loss in activity after startup (27). After each experiment, the catalyst was reduced in D_2/He at 543 K for 2 h, to ensure that steady-state activity levels were maintained.

Isotopic-tracer, transient-response experiments were initiated by switching the feed from a stream containing ^{12}CO to one containing an equivalent concentration of ^{13}CO, after steady-state conditions had first been achieved in ^{12}CO. In this fashion, the steady-state activity of the catalyst was not perturbed by the switch in isotopic label on the CO. To obtain good temporal resolution of the isotopic composition of the products, the following sampling sequence was used. Samples were taken just prior to and 15 s after the switch in CO isotopic composition, followed by four samples taken at 10 s intervals, followed by five samples taken after intervals of 15, 20, 30, 120, and 240 s, respectively. In this way, 11 samples were acquired in 8 min. After the first series of samples, the feed was switched from a mixture of ^{13}CO and D_2 in He to one containing ^{12}CO and D_2 in He and the reaction allowed to proceed in this later mixture for 15 min. The feed composition was then changed back again from $^{12}CO/D_2$/He to $^{13}CO/D_2$/He and three samples were taken at 10-s intervals after the last of which one more sample was taken following an interval of 30 s. Because the fill-time of the sample loops is 6 s, data were not collected at intervals shorter than 10 s.

Figure 1 illustrates the sampling procedure described above. In this figure, $F_n(t)$ represents the fraction of ^{13}C-labeled products containing n carbon numbers. Since the transients for olefinic and paraffinic products of a given carbon number were identical, the data for all products with a given carbon number were combined. It was also observed that the transients during each sampling period were highly reproducible for a given set of reaction condi-

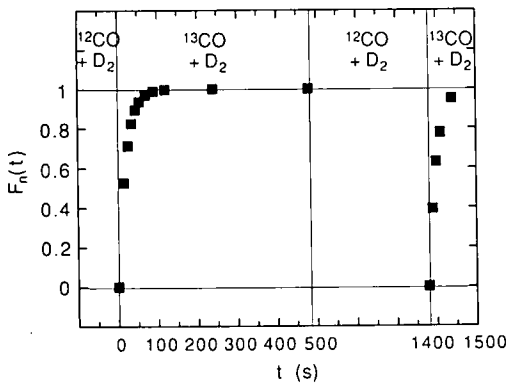

FIG. 1. Data sampling sequence for isotopic transients.

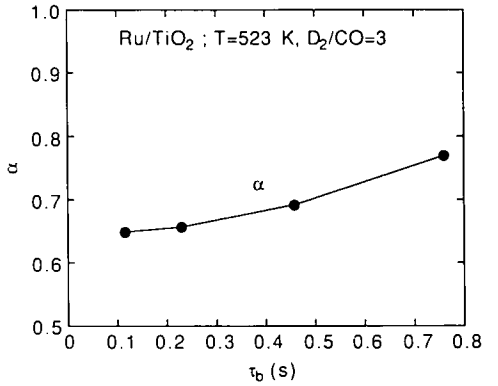

FIG. 3. Chain growth probability as a function of catalyst bed residence time.

tions and, consequently, the data for the first and second sampling periods were combined into one transient consisting of 15 data points.

RESULTS

Figure 2 shows the effects of catalyst bed residence time τ_b (the ratio of the catalyst bed volume to the volumetric flowrate of the feed mixture) on the turnover frequencies for total CO consumption and the formation of methane. For the conditions indicated, the conversion of CO varies from 7–35% as τ_b increases from 0.12 to 0.76 s. With increasing catalyst-bed residence time, the turnover frequency for CO consumption decreases by about a factor of 1.5, but that for the formation of methane decreases by a factor of 2.5. The observed decrease in the selectivity to methane with increasing catalyst-bed residence time is accompanied by an increase in the probability for chain growth, α, as can be seen in Fig. 3.

The influence of catalyst-bed residence time on the turnover frequency for the formation of α-olefins and normal paraffins of a given carbon number are presented in Figs. 4 and 5. Figure 4 shows a nearly fourfold decrease in the turnover frequency for ethylene formation with increasing catalyst-bed residence time, whereas the turnover frequency for ethane formation is not strongly affected. The effects of catalyst-bed residence time on C_{3+} hydrocarbons are illustrated by the data shown in Fig. 5 for $n = 4$. Here again, increasing catalyst-bed residence time causes a decrease in the turnover frequency for the formation of the olefin, but now an increase is observed in the turnover frequency for the formation of the paraffin.

Isotope-ratio GC–MS was used to monitor the incorporation of ^{13}C in C_{2-8} products, following a switch in the feed from ^{12}CO/D$_2$ to ^{13}CO/D$_2$. Figures 6 and 7 show representative curves of $F_n(t)$ for the cases of $\tau_b = 0.23$ and 0.46 s. The data presented in these figures are based on the measured isotopic fractions in all olefins and paraffins of a given carbon number, since it was observed that the dynamics for products with a given number of carbon atoms could not be differentiated on the basis of structure (e.g., olefin vs paraffin). It is evident from these figures

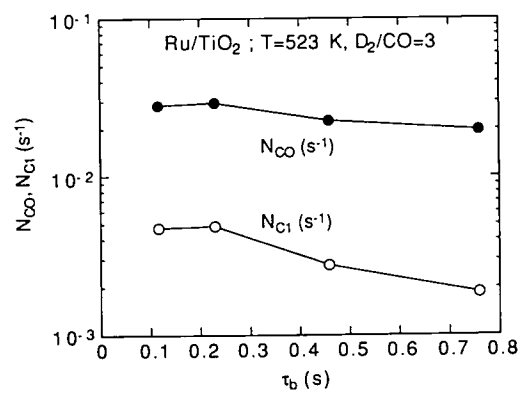

FIG. 2. Turnover frequencies for CO consumption and methane formation as a function of catalyst bed residence time.

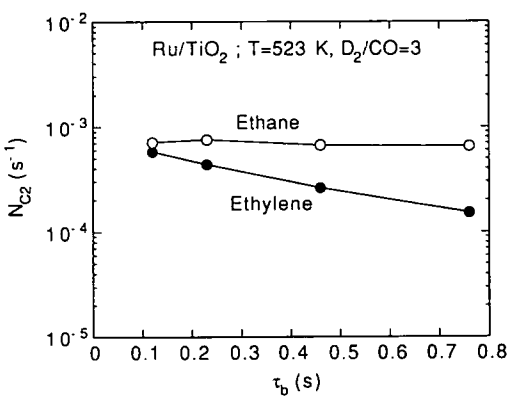

FIG. 4. Turnover frequencies for ethylene and ethane formation as a function of catalyst bed residence time.

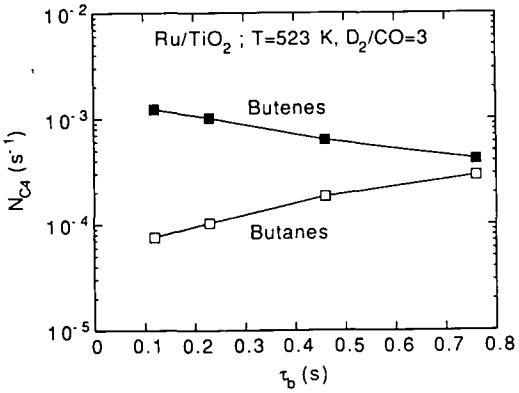

FIG. 5. Turnover frequencies for butene and butane formation as a function of catalyst bed residence time.

that for a given catalyst-bed residence time, the curves of $F_n(t)$ rise progressively more slowly the larger the value of n. This trend is suggestive of a stepwise polymerization process. More surprising is the observation that for a given carbon number, $F_n(t)$ rises more slowly the longer the catalyst-bed residence time.

For the purposes of data interpretation (see below) it

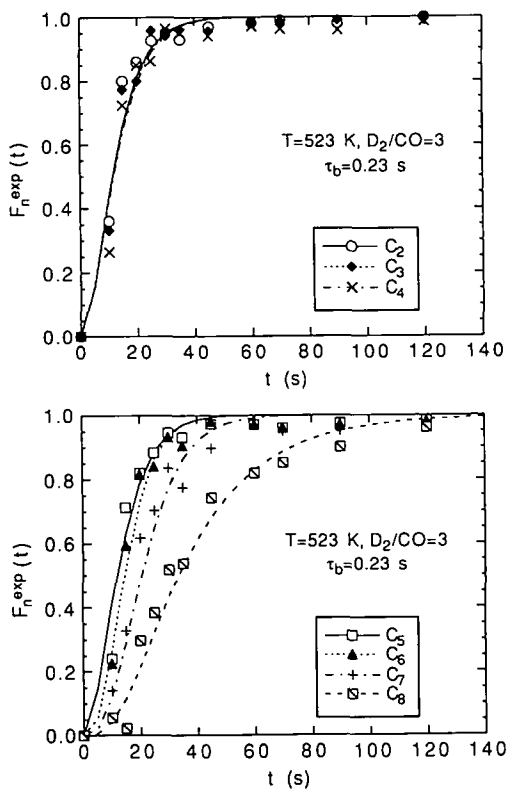

FIG. 6. Fractional content of ^{13}C in C_{3-5} and C_{6-8} products as a function of time for τ_b = 0.12 s.

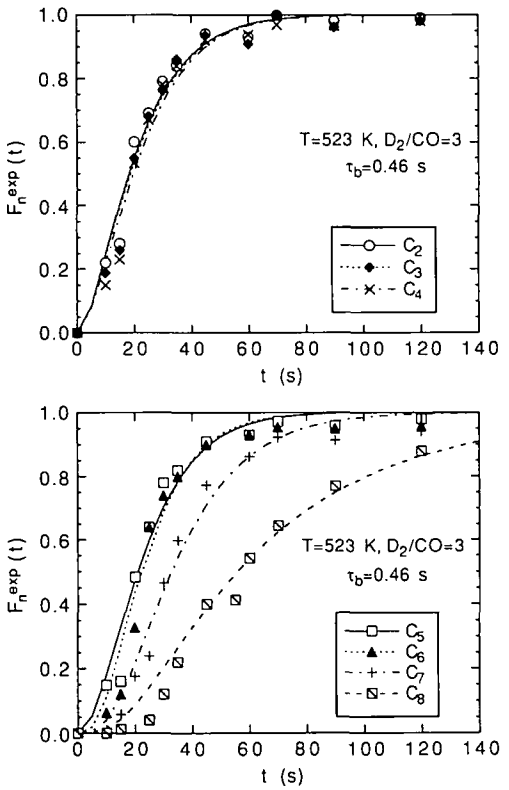

FIG. 7. Fractional content of ^{13}C in C_{3-5} and C_{6-8} products as a function of time for τ_b = 0.76 s.

was important to establish whether or not condensation of any part of the hydrocarbon products occurred in the pores of the catalyst and the extent to which intraparticle mass transfer might influence both the steady-state and transient-response rates. From an analysis of the BET isotherm of the catalysts it was established that the mean pore diameter is 20 nm and that there is no significant pore volume for pores with diameters less than 2 nm. From the Kelvin equation it was determined that for the reaction conditions used, the partial pressures of C_{2+} products over the catalyst are three orders of magnitude or more smaller than the partial pressure required for condensation in even the smallest pores. The time constant for intraparticle diffusion was estimated from the average particle diameter 0.2 mm and the magnitude of the Knudsen diffusion coefficient for each product. From these calculations it was concluded that the time constant for diffusion is a minimum of one to two orders of magnitude smaller than the time constant for the formation of hydrocarbon products. As a consequence, it is safe to conclude that neither capillary condensation nor intraparticle mass transfer affects the results presented in Figs. 2–7.

DISCUSSION

Steady-State Results

It is evident from Figs. 2–5 that the catalyst-bed residence time affects not only the steady-state turnover frequency for CO consumption but also the probability of chain growth, the turnover frequency for methane formation, and the turnover frequencies for the formation of olefins and paraffins of a given carbon number. Each of these effects can be attributed to readsorption of olefins (13, 14, 17–19). As noted in the Introduction, previous studies have shown that the readsorption of ethylene is much more rapid than that of other olefins. This process leads to an enhanced concentration of adsorbed ethyl groups which can act as C_2 chain initiators and provide CH_2 and CH_3 species via depolymerization. The decrease in N_{C1} and the increase in α with increasing τ_b are both attributable to the enhanced rate of chain initiation caused by the readsorption of ethylene (13, 17–19). The observed decrease in the turnover frequency of ethylene formation and the near independence of the turnover frequency for ethane formation, seen in Fig. 4, show that very little of the readsorbed ethylene undergoes hydrogenation to form ethane, in good agreement with what has been reported previously. By contrast, C_{3+} olefin readsorption leads largely to the formation of the corresponding paraffin. This behavior is evident from the data presented in Fig. 5, which show that the turnover frequency for butane formation nearly completely compensates for the decrease in turnover frequency for butene formation as τ_b increases.

Chain Growth Model

The chain growth scheme shown in Fig. 8 is used as the basis for simulating the experimentally observed transients. This model is based on extensive physical evidence (cf., Refs. (1–19)) and is similar to that described previously by Krishna and Bell (24) but takes into account the effects of olefin readsorption and ethylene depolymerization. Steps leading to the progressive deactivation of Ru by C_β carbon are not included in the scheme because the dynamics of deactivation via this mechanism are much slower than those of the reactions leading to products (27). For example, for the reaction conditions studied the longest time constant associated with the transient response curves is of the order 1 min, whereas the time constant for the accumulation of C_β carbon is of the order of 100 min.

In Fig. 8, CO_g and CO_s refer to gas-phase and adsorbed CO, $C_{m,s}$ refers to adsorbed monomeric building units, and $C_{n,s}$ and $C_{n,g}$ refer to adsorbed alkyl chains and gaseous products containing n carbon atoms. The conversion of adsorbed CO to $C_{m,s}$ appears as a single elementary step, but in fact it occurs via a sequence of steps, consisting of the dissociation of CO_s, followed by stepwise hydrogenation of the nascent carbon to $CH_{1,s}$ and $CH_{2,s}$ species (1–3, 5). Chain growth is initiated by the hydrogenation of $CH_{2,s}$ species to form $CH_{3,s}$ species. Chain propagation proceeds via the stepwise addition of $CH_{2,s}$ groups to adsorbed alkyl groups. For the chain termination step no distinction is made between chain termination to olefins and paraffins. In contrast to the model proposed Krishna and Bell (24), desorption of C_n products into the gas phase is assumed to be mediated by a physisorbed precursor (28). Reentry of the olefins from the physisorbed state is also allowed to occur, as is depolymerization of $C_{2,s}$ species and the conversion of $C_{1,s}$ species to $C_{m,s}$ species. The rate coefficient for conversion of $C_{m,s}$ to $C_{1,s}$ is the apparent first-order rate coefficient for chain initiation, k_i, and the rate coefficient for the reverse of this process is k_{ir}. The rate coefficients k_p and k_t are first-order rate coefficients for chain propagation and termination. The rate coefficients k_{dp} and k'_{re} characterize the rate of depolymerization of ethyl groups and the rate of their formation by reentry of ethylene from the physisorbed state. The rate of reentry of C_{3+} olefins from the physisorbed state is characterized by k_{re}. The dependence of any process on adsorbed hydrogen is not shown explicitly, since, for a given set of reaction conditions, the surface coverage of hydrogen is time independent.

Steady-State and Label Balances

Expressions can readily be derived for $F_m(t)$, $F_n(t)$, and $F_n^{ps}(t)$, the fraction of labeled carbon in the monomer pool, the pool of alkyl chain containing n carbon atoms, and the pool of physisorbed products containing n carbon atoms, respectively. No account is taken of the possible variations in the concentrations of species along the reactor axis, which is equivalent to assuming that the reactor behaves as a CSTR. This assumption is reasonably valid for $0.12 \leq \tau_b \leq 0.43$ s.

A mass balance on labeled carbon entering and leaving the monomer pool gives

$$\theta_m \frac{dF_m}{dt} = k_d \theta_{CO} F_{CO} - \theta_m (k_i + k_p \sum_{n=1}^{\infty} \theta_n) F_m + k_{ir} \theta_1 F_1 + k_{dp} \theta_2 F_2. \quad [1]$$

In Eq. [1], θ_{CO}, θ_m, and θ_n are the surface coverages for CO, monomeric building units, $C_{m,s}$ and alkyl chain, $C_{n,s}$, respectively. At steady state,

$$N_{CO} = k_d \theta_{CO} = \theta_m (k_i + k_p \sum_{n=1}^{\infty} \theta_n) - k_{ir} \theta_1 - k_{dp} \theta_2. \quad [2]$$

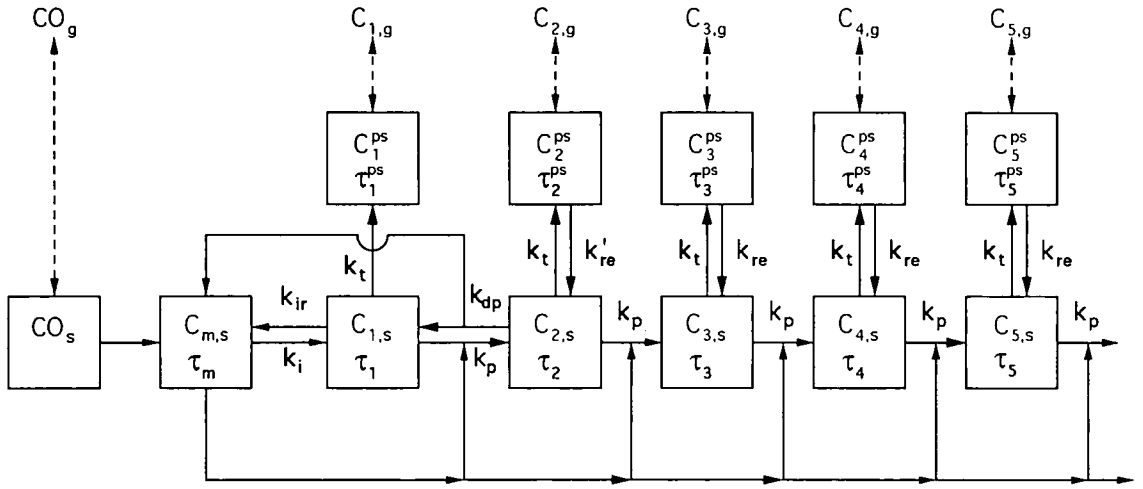

$$\frac{1}{\tau_m} = (k_i + k_p \sum_{n=1}^{\infty} \theta_n) - k_{ir}\left(\frac{\theta_1}{\theta_m}\right) - k_{dp}\left(\frac{\theta_2}{\theta_m}\right) \qquad \frac{1}{\tau_1} = (k_t + k_p\theta_m) + k_{ir} - k_{dp}\left(\frac{\theta_2}{\theta_1}\right)$$

$$\frac{1}{\tau_2} = (k_t + k_p\theta_m) - k'_{re}\left(\frac{\theta_{2=}^{ps}}{\theta_2}\right) + k_{dp} \qquad \frac{1}{\tau_n} = (k_t + k_p\theta_m) - k_{re}\left(\frac{\theta_{n=}^{ps}}{\theta_n}\right)$$

$$\frac{1}{\tau_n^{ps}} = k_{re}\left(\frac{\theta_{n=}^{ps}}{\theta_n^{ps}}\right) + \left(\frac{Q}{WK_nRT}\right) \qquad \alpha_n = \frac{k_p\theta_m}{(k_p\theta_m + k_t - k_{re}(\frac{\theta_{n=}^{ps}}{\theta_n}))}$$

FIG. 8. Chain growth model.

Combining Eqs. [1] and [2], one obtains

$$\frac{dF_m}{dt} = (k_i + k_p \sum_{n=1}^{\infty} \theta_n)(F_{CO} - F_m) - k_{ir}\left(\frac{\theta_1}{\theta_m}\right)(F_{CO} - F_1) - k_{dp}\left(\frac{\theta_2}{\theta_m}\right)(F_{CO} - F_2) \quad [3]$$

On the assumption that F_1 and F_2 are nearly equal to F_m, Eq. [3] can be rewritten as

$$\frac{dF_m}{dt} = \frac{(F_{CO} - F_m)}{\tau_m}, \quad [4]$$

where $1/\tau_m = (k_i + k_p \Sigma_n \theta_n) - k_{ir}(\theta_1/\theta_m) - k_{dp}(\theta_2/\theta_m)$.

The appearance and disappearance of labeled carbon in the methane precursor pool C_1 is governed by

$$\theta_1\frac{dF_1}{dt} = k_i\theta_m F_m - \theta_1 F_1(k_t + k_p\theta_m) - k_{ir}\theta_1 F_1 + k_{dp}\theta_2 F_2. \quad [5]$$

Since at steady state

$$k_i\theta_m = \theta_1(k_t + k_p\theta_m) + k_{ir}\theta_1 - k_{dp}\theta_2, \quad [6]$$

Eq. [5] can be rewritten as

$$\frac{dF_1}{dt} = (k_t + k_p\theta_m + k_{ir})(F_m - F_1) - k_{dp}\left(\frac{\theta_2}{\theta_1}\right)(F_m - F_2). \quad [7]$$

If F_2 is nearly equal to F_1, Eq. [7] can be simplified to

$$\frac{dF_1}{dt} = \frac{(F_m - F_1)}{\tau_1}, \quad [8]$$

where $1/\tau_1 = (k_t + k_p\theta_m) + k_{ir} - k_{dp}(\theta_2/\theta_1)$.

In a similar manner, a balance on the precursors to C_2 products gives

$$2\theta_2\frac{dF_2}{dt} = k_p\theta_m\theta_1(F_1 + F_m) - 2(k_t + k_p\theta_m)\theta_2 F_2 + 2k'_{re}\theta_{2=}^{ps}F_2^{ps} - 2k_{dp}\theta_2 F_2, \quad [9]$$

where $\theta_{2^=}^{ps}$ is the coverage of physisorbed ethylene. At steady state

$$k_p\theta_1\theta_m = (k_t + k_p\theta_m)\theta_2 - k'_{re}\theta_{2^=}^{ps} + k_{dp}\theta_2. \quad [10]$$

Substituting Eq. [10] into Eq. [9] and introducing the assumption that $F_2^{ps} = F_2$ results in

$$\frac{dF_2}{dt} = \left(\frac{F_1 + F_m}{2} - F_2\right)\Big/\tau_2, \quad [11]$$

where $1/\tau_2 = (k_t + k_p\theta_m) - k'_{re}(\theta_{2^=}^{ps}/\theta_2) + k_{dp}$.

The balance on labeled carbon in the pool of alkyl species containing n carbon atoms is given by

$$n\theta_n\frac{dF_n}{dt} = k_p\theta_m\theta_{n-1}[(n-1)F_{n-1} + F_m] - n(k_t + k_p\theta_m)\theta_n F_n + nk_{re}\theta_{n^=}^{ps}F_{n^=}^{ps}. \quad [12]$$

In Eq. [12], $\theta_{n^=}^{ps}$ is the coverage of physisorbed olefins. The material balance at steady state is

$$k_p\theta_m\theta_{n-1} = (k_t + k_p\theta_m)\theta_n - k_{re}\theta_{n^=}^{ps}. \quad [13]$$

Substituting Eq. [13] into Eq. [12], one obtains

$$\frac{dF_n}{dt} = \left(\frac{(n-1)F_{n-1} + F_m}{n}\right)\Big/\tau_n - \frac{F_n}{\tau} + \frac{F_n^{ps}}{\tau_{re,n}}, \quad [14]$$

where $1/\tau_n = (k_t + k_p\theta_m) - k_{re}(\theta_{n^=}^{ps}/\theta_n) = 1/\tau - 1/\tau_{re,n}$. The balance on labeled carbon in the pool of physisorbed products is given by

$$n\theta_n^{ps}\frac{dF_n^{ps}}{dt} = k_t\theta_n(nF_n) - k_{re}\theta_{n^=}^{ps}(nF_n^{ps}) - \frac{QP_n}{Wn_{Ru}RT}(nF_n^{ps}). \quad [15]$$

In Eq. [15], θ_n^{ps} is the coverage of physisorbed products containing n carbon atoms, P_n/RT is the gas-phase concentration of products containing n carbon atoms, Q is the volumetric flow rate of gas, W is the weight of catalyst, and n_{Ru} is the concentration of exposed Ru atoms per weight of catalyst. The partial pressure P_n can be related to θ_n^{ps} by a Henry's law expression, so that

$$P_n = \theta_n^{ps}n_{Ru}/K_n, \quad [16]$$

where K_n is the Henry's law constant. A material balance on the physisorbed material gives

$$k_t\theta_n = k_{re}\theta_{n^=}^{ps} + \left(\frac{QP_n}{Wn_{Ru}RT}\right). \quad [17]$$

Substitution of Eqs. [16] and [17] into Eq. (15) gives

$$\frac{dF_n^{ps}}{dt} = \frac{(F_n - F_n^{ps})}{\tau_n^{ps}}, \quad [18]$$

where $1/\tau_n^{ps} = k_{re}(\theta_{n^=}^{ps}/\theta_n^{ps} + Q/WK_nRT) = 1/\tau_{re,n}^{ps} + 1/\tau_{cv}^{ps}$.

The initial conditions on F_m and $F_n(n = 1\text{–}8)$ are $F_m = F_n = 0$ at $t = 0$. Since CO is assumed to equilibrate rapidly with the catalyst surface, $F_{CO} = 1$ for $t \geq 0$. With these initial conditions, the solution to Eq. [4] is

$$F_m(t) = 1 - \exp(-t/\tau_m) \quad [19]$$

and the solution to Eq. [11] is

$$F_2(t) = 1.0 + \frac{1}{2}\exp\left(-\frac{t}{\tau_m}\right)\left[\left(\frac{\tau_m}{\tau_2 - \tau_m}\right) - \left(\frac{\tau_m}{\tau_2 - \tau_m}\right)^2\right] + \frac{1}{2}\exp\left(-\frac{t}{\tau_2}\right)\left[\left(\frac{\tau_m}{\tau_2 - \tau_m}\right)^2 - \left(\frac{\tau_2}{\tau_2 - \tau_m}\right) - \left(\frac{t}{\tau_2 - \tau_m}\right) - 1\right]. \quad [20]$$

in solving Eq. [11] it is assumed that F_2 is approximately equal to F_1.

Two different approaches are used to solve for $F_n(t)$ and $F_n^{ps}(t)$. For $n = 3\text{–}5$, it is assumed that $F_n^{ps} = F_n$ (which is equivalent to assuming that $\tau_{re,n} \gg \tau$ and, hence, that $\tau_n = \tau$) so that the last two terms of Eq. [14] can be combined. Under these circumstances Eq. [14] can be solved by the method of Laplace transforms to obtain

$$F_n(t) = 1.0 + \left(\frac{\exp(-t/\tau_m)}{n}\right)\left[\sum_{i=1}^{n-2}(-1)^{i-1}\left(\frac{\tau_m}{\tau - \tau_m}\right)^i + (-1)^{n-2}\left(\frac{\tau_m}{\tau - \tau_m}\right)^{n-2}\left(\frac{\tau_m}{\tau_2 - \tau_m}\right) + (-1)^{n-1}\left(\frac{\tau_m}{\tau - \tau_m}\right)^{n-2}\left(\frac{\tau_m}{\tau_2 - \tau_m}\right)^2\right] + \left(\frac{\exp(-t/\tau)}{n}\right) \times \left[\sum_{i=1}^{n-2}\frac{1}{\tau^i}\sum_{r=0}^{i-1}\frac{t^{i-r-1}}{(i-r-1)!}\tau^{r+1}\left(\left(-\frac{\tau_m}{\tau - \tau_m}\right)^{r+1} - 1\right) + \frac{1}{\tau_2}\sum_{i=1}^{n-2}\frac{1}{\tau^{i-1}}\left(\left(-\frac{\tau_m}{\tau - \tau_m}\right)^{n-i-1} - 1\right) \times \sum_{r=0}^{i-1}(-1)^r\frac{t^{i-r-1}}{(i-r-1)!}\tau^{r+1}\left(\frac{\tau_2}{\tau - \tau_2}\right)^{r+1} + \frac{1}{(\tau_2)^2}\sum_{i=1}^{n-2}\frac{1}{\tau^{i-1}}\left(\left(-\frac{\tau_m}{\tau - \tau_m}\right)^{n-i-1} - 1\right)$$

$$\times \left\{ t \sum_{r=0}^{i-1} (-1)^r \frac{t^{i-r-1}}{(i-r-1)!} \tau^{r+1} \left(\frac{\tau_2}{\tau-\tau_2}\right)^{r+1} \right. \quad [21]$$

$$\left. - \sum_{r=0}^{i} (-1)^r i \frac{t^{i-r}}{(i-r)!} \tau^{r+1} \left(\frac{\tau_2}{\tau-\tau_2}\right)^{r+1} \right\} \Bigg]$$

$$- \left(\frac{\exp(-t/\tau_2)}{n}\right) \left[2 + (-1)^{n-2} \left(\frac{\tau_m}{\tau-\tau_m}\right)^{n-2} \left(\frac{\tau_m}{\tau_2-\tau_m}\right) \right.$$

$$+ (-1)^{n-1} \left(\frac{\tau_m}{\tau-\tau_m}\right)^{n-2} \left(\frac{\tau_m}{\tau_2-\tau_m}\right)^2$$

$$+ \left(\frac{t}{\tau_2}\right) \left\{ 1 + (-1)^{n-2} \left(\frac{\tau_m}{\tau-\tau_m}\right)^{n-2} \left(\frac{\tau_m}{\tau_2-\tau_m}\right) \right\}$$

$$+ \left(\frac{1}{\tau_2} + \frac{t}{(\tau_2)^2}\right) \sum_{i=1}^{n-2} \left(\left(-\frac{\tau_m}{\tau-\tau_m}\right)^{n-i-1} - 1 \right)$$

$$\times (-1)^{i-1} \tau \left(\frac{\tau_2}{\tau-\tau_2}\right)^i - \frac{1}{(\tau_2)^2} \sum_{i=1}^{n-2}$$

$$\left. \times \left(\left(-\frac{\tau_m}{\tau-\tau_m}\right)^{n-i-1} - 1 \right) (-1)^i \tau^2 \left(\frac{\tau_2}{\tau-\tau_2}\right)^{i+1} \right].$$

For n = 6–8 the assumption that $F_n^{ps} - F_n$ is no longer valid (see below), and, hence, it becomes necessary to solve Eq. [18] in order to compare the simulated transients with those observed experimentally. Since the form of Eq. [21] is too complex for this purpose, further simplifications must be made. The first step is to assume that an adequate approximation for F_n can be obtained by solving Eq. [14] under the assumption that $\tau_1 = \tau_2 = \tau$. This leads to the following expression for $F_n(t)$, which is identical to that presented previously by Krishna and Bell (24):

$$F_n(t) = 1.0 + \left(\frac{\exp(-t/\tau_m)}{n}\right) \sum_{i=1}^{n-1} (-1)^{i-1} \left(\frac{\tau_m}{\tau-\tau_m}\right)^i$$

$$+ \left(\frac{\exp(-t/\tau)}{n}\right) \sum_{i=1}^{n-2} \frac{1}{\tau^i} \sum_{r=0}^{i-1} \frac{t^{i-r-1}}{(i-r-1)!} \tau^{r+1} \quad [22]$$

$$\times \left(\left(-\frac{\tau_m}{\tau-\tau_m}\right)^{r+1} - 1 \right).$$

Substitution of Eq. [22] into Eq. [18] and solution of the latter equation results in

$$F_n^{ps}(t) = 1.0 + \left(\frac{\exp(-t/\tau_m)}{n}\right) \left(\frac{\tau_m}{\tau_m - \tau_n^{ps}}\right) \sum_{i=1}^{n} (-1)^{1-i}$$

$$\times \left(\frac{\tau_m}{\tau-\tau_m}\right)^i + \left(\frac{\exp(-t/\tau)}{n}\right) \frac{1}{\tau_n^{ps}} \sum_{i=1}^{n} \tau^{-i+1} \sum_{q=0}^{n-i}$$

$$\left(\left(-\frac{\tau_m}{\tau-\tau_m}\right)^{q+1} - 1 \right) \sum_{r=0}^{i-1} (-1)^r \frac{t^{i-r-1}}{(i-r-1)!}$$

$$\times \left(\frac{\tau_n^{ps}\tau}{\tau-\tau_n^{ps}}\right)^{r+1} - \left(\frac{\exp(-t/\tau_n^{ps})}{n}\right) \left[n + \left(\frac{\tau_m}{\tau_m-\tau_n^{ps}}\right) \right.$$

$$\sum_{i=1}^{n} (-1)^{i-1} \left(-\frac{\tau_m}{\tau-\tau_m}\right)^i + \frac{\tau}{\tau_n^{ps}} \sum_{i=1}^{n} (-1)^{i-1}$$

$$\left. \times \left(\frac{\tau_n^{ps}}{\tau-\tau_n^{ps}}\right)^i \sum_{q=0}^{n-i} \left(\left(-\frac{\tau_m}{\tau-\tau_m}\right)^{q+1} - 1 \right) \right]. \quad [23]$$

Determination of Rate Coefficients and Surface Coverages

Values of the parameters τ_m, τ_2, τ_n, and τ_n^{ps} were obtained by fitting the analytical expressions for F_n (n = 2–5) or F_n^{ps} (n = 6–8) given by Eqs. [21] and [23], respectively, to the experimental data obtained for a given catalyst bed residence time. This was done by using a quasi-Newton method (29) to minimize the objective functions $S_n(\tau_m, \tau_2, \tau)$ and $S_n(\tau_m, \tau, \tau_n^{ps})$ defined as

$$S_n(\tau_m, \tau_2) = \sum_{j=1}^{M} [F_n^{exp}(t_j) - F_n(t_j)]^2, \quad \text{for } n = 2, \quad [24]$$

$$S_n(\tau_m, \tau_2, \tau) = \sum_{j=1}^{M} [F_n^{exp}(t_j) - F_n(t_j)]^2, \quad \text{for } n = 3\text{–}5, \quad [25]$$

and

$$S_n(\tau_m, \tau, \tau_n^{ps}) = \sum_{j=1}^{M} [F_n^{exp}(t_j) - F_n^{ps}(t_j)]^2, \quad \text{for } n = 6\text{–}8. \quad [26]$$

In Eqs. [24]–[26], $F_n^{exp}(t_j)$ is the experimental value of the fractional degree of labeling at time t_j and M is the number of experimental points.

The curves in Figs. 6 and 7 show the best fit of the transient response model to the data. The F-test was used to assess the statistical adequacy or lack of fit of the model [30]. For each value of n, the F-test indicated that the model fit the data at a 95% confidence interval.

Since different functional forms of $F_n(t)$ were used to represent the data for n = 2–5 and n = 6–8, a check was carried out to determine the consistency of Eqs. [21] and [22]. For a fixed set of rate coefficients (see Table 1 below), the values of $F_n(t)$ for n = 6–8 obtained from Eqs. [21] and [22] never deviate by more than 5% over the interval $0 < t < 140$ s, for $\tau_b = 0.12$ and 0.23 s, and for $\tau_b > 0.23$ s, the deviation between the two solutions is less than 5% on average.

The values of individual rate coefficients and the coverages of the catalyst surface by monomeric species and growing alkyl chains were determined from the values of τ_m, τ_2, τ, and τ_n^{ps} obtained through the fitting procedure described above, and the values of N_{CO}, N_{C_n}, and α obtained from steady-state rate data. The approach used to

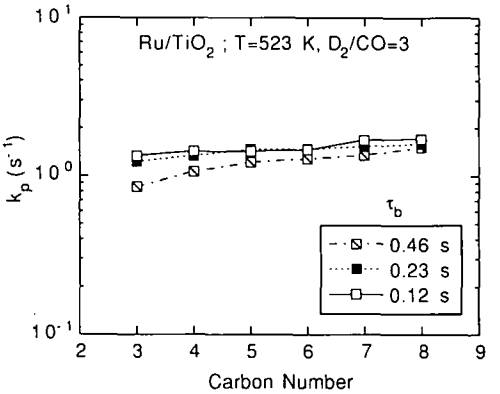

FIG. 9. Values of k_p versus carbon number for different catalyst-bed residence times.

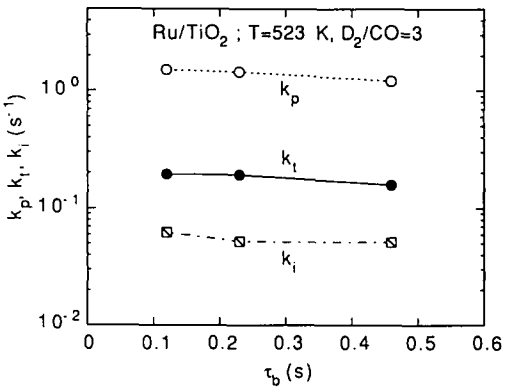

FIG. 11. Values of k_i, k_p, and k_t as a function of catalyst-bed residence time.

calculate rate coefficients and surface coverages is detailed in the Appendix.

Figures 9 and 10 show plots of k_p and k_t versus carbon number determined using the procedure described above. It is evident that both rate coefficients are virtually independent of n, particularly for low values of τ_b, for which the assumptions used to develop the expressions for F_n and F_n^{ps} are most valid. The slight decrease in k_t and k_p with decreasing carbon number, particularly for high values of τ_b, might be caused by the modest effect of the reincorporation of propylene. Figure 11 shows that k_i, and the average values of k_p and k_t, are independent of the catalyst-bed residence time. The independence of k_p and k_t on n, and the independence of k_i, and the average values of k_p and k_t on τ_b represent stringent tests of the validity of the scheme shown in Fig. 8 for describing the dynamics of chain initiation, propagation, and termination. It should be noted that attempts to simulate the transient-response curves shown in Figs. 6 and 7 using a scheme which neglected olefin readsorption and the depolymerization of ethylene resulted in values of k_p and k_t which passed through a maximum with increasing n and decreased with increasing τ_b.

In view of the relatively small separation between the curves of $F_n(t)$ for $n = 2$–5, the accuracy of the estimates of K_p and k_t were carefully examined. As shown in the Appendix, k_p and k_t are given by

$$k_p = \alpha/(N_{CO}\tau_m\tau) \quad \text{and} \quad k_t = (1-\alpha)/\tau. \qquad [27]$$

Since the values of N_{CO} and α can be determined to a high degree of accuracy from the steady-state data and the value of τ_m is constant for all values of n, the accuracy of k_p and k_t is dictated by the accuracy with which τ can be determined. An investigation of the sensitivity of the fits to the experimentally observed transients in $F_n(t)$ for $n = 3$–5 showed that τ can be determined with an accuracy of ±50%. This means that the values of k_p and k_t shown in Figs. 9 and 10 are accurate to within a factor of about two.

The values of k_{ir}, k_{dp}, k_{re}, and k'_{re} are listed in Table 1. Also shown for comparison are the values of k_i, and the average values of k_p and k_t. Of particular note is the fact that the value of k'_{re} is approximately four orders of magnitude larger than the value of k_{re}, suggesting that ethylene should reenter the chain growth process much more rapidly than higher molecular weight olefins. This point is discussed in more detail below. The values of k_p and k_t listed in Table 1 agree very closely with the values reported recently by Krishna and Bell (24), when their data

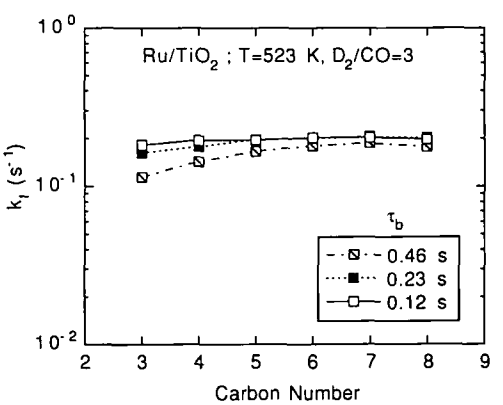

FIG. 10. Values of k_t versus carbon number for different catalyst bed residence times.

TABLE 1

Summary of Rate Coefficients

$k_i = 0.05\ s^{-1}$	$k_{ir} = 0.20\ s^{-1}$
$k_p = 1.40\ s^{-1}$	$k_{dp} = 0.31\ s^{-1}$
$k_t = 0.18\ s^{-1}$	$k_{re} = 0.015\ s^{-1}$
$k'_{re} = 150\ s^{-1}$	

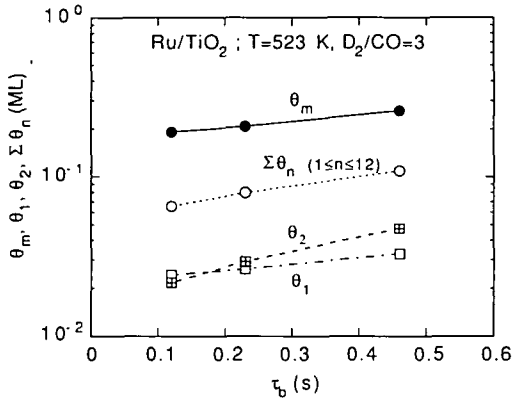

FIG. 12. Values of θ_m, θ_1, θ_2, and $\Sigma\theta_n$ as a function of catalyst-bed residence time.

are extrapolated to 523 K. The value of k_i in Table 1 is a factor of 2.5 larger than that reported by Krishna and Bell. The difference between the values of k_i are not fully understood but are thought to be attributable to differences in manner of catalyst preparation, Ru dispersion, and the method of data analysis in the two studies.

The values of θ_m, θ_1, θ_2 and $\Sigma\theta_n$ are shown in Fig. 12 as a function of τ_b. The modest rise in the coverages by intermediates in the chain growth process can be attributed to an increasing in the degree of ethylene readsorption with increasing catalyst bed residence time, as a consequence in the rise of in the partial pressure of ethylene.

The results presented in Table 1 and Fig. 12 can be used to draw a number of deductions concerning the relative rates of various processes involved in the formation of products during FTS. Figure 13 shows that the rate of C_{3-8} olefin reincorporation is significantly smaller than the rate of chain termination, particularly at low catalyst-bed

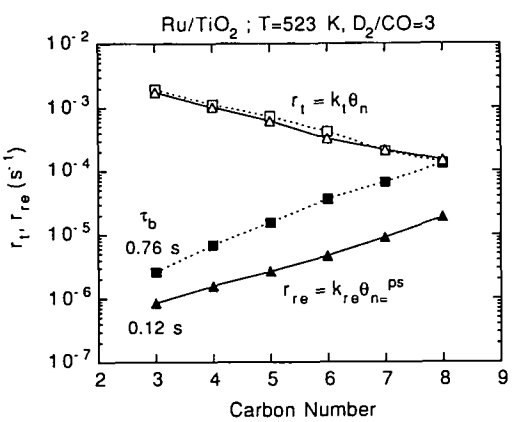

FIG. 13. Comparison of the r_t and r_{re} for different carbon numbers.

TABLE 2

Rates of Reaction for Elementary Processes Involving Ethylene

$CH_{2,s} + H_s \rightleftharpoons CH_{3,s}$	$r_i = 1.0 \times 10^{-2}\ s^{-1}$	$r_{ir} = 4.9 \times 10^{-3}\ s^{-1}$
$CH_{3,s} + CH_{2,s} \rightleftharpoons C_2H_{5,s}$	$r_p = 6.4 \times 10^{-3}\ s^{-1}$	$r_{dp} = 5.8 \times 10^{-3}\ s^{-1}$
$C_2H_{5,s} \rightleftharpoons H_s + C_2H_{4,ps}$	$r_t = 3.4 \times 10^{-3}\ s^{-1}$	$r_{re} = 2.4 \times 10^{-3}\ s^{-1}$

residence time, consistent with the assumptions used in deriving the expressions for F_n and F_n^{ps}. In strong contrast to the case for C_{3+} products, Fig. 13 and Table 2 show that the rate of C_2 reincorporation is comparable to the rate of C_2 product formation. The rate of $C_{2,s}$ depolymerization is nearly the same as the rate of $C_{2,s}$ formation chain propagation. Interestingly, Table 2 reveals that the rate of methyl group dehydrogenation to form a methylene group is approximately 50% of the rate of chain initiation. Two other deductions that can be drawn from Table 2 are that the rate of C_2 chain termination is roughly half as fast as the rates of $C_{2,s}$ depolymerization, and that the rate of chain initiation is approximately four times higher than the rate of chain initiation resulting from the readsorption of ethylene to form $C_2H_{5,s}$ species. The much higher rate of ethylene reentry into the chain growth process compared to higher molecular weight olefins is completely consistent with experimental observation (13, 14, 18, 19).

The increase in response time of the experimental data for $F_n(t)$ with increasing catalyst-bed residence time seen in Figs. 6 and 7 can be attributed to several causes. For $n = 2$–5, feedback of unlabeled carbon due to rapid ethylene readsorption and depolymerization causes the value of τ_m, τ_1, and τ_2 to increase with τ_b. The increase in τ_m, in turn, causes an increase in the time it takes the experimental values of $F_n(t)$ to approach unity. For $n = 6$–8, the delay in the approach of the transient response curves to unity is attributable primarily to the increase in the values of τ_n^{ps} with τ_b. It is recalled that the value of τ_n^{ps} is comprised of two parts (see Eq. [18], one due to readsorption of C_n olefins from the physisorbed layer and the other due to removal of physisorbed hydrocarbons as a consequence of convection. Figure 14 shows that for small and large values of τ_b, the convective term is the dominant contributor to τ_n^{ps} for values of $n \leq 8$. For values of n greater than 8, the readsorption of olefins from the physisorbed layer becomes progressively more important. It is also evident from Fig. 14 that for $n \leq 6$, $k_t \gg 1/\tau_n^{ps}$, whereas for $n \geq 7$, $k_t \ll 1/\tau_n^{ps}$. These results are consistent with the assumption that for $n = 6$–8, the dynamics of exchanging ^{13}C-labeled hydrocarbons from the physisorbed layer on the catalyst surface must be taken into account in simulating the experimentally observed curves of $F_n(t)$.

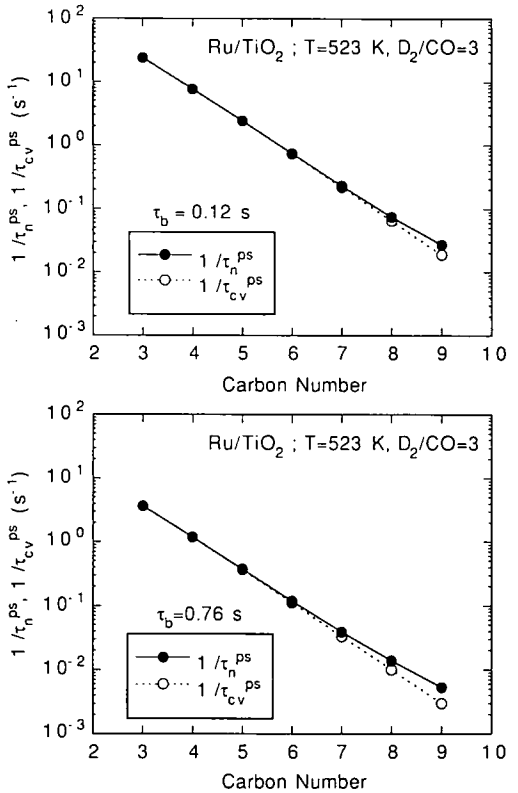

FIG. 14. The effect of carbon number on $(1/\tau_n^{ps})$ and $(1/\tau_{cv}^{ps})$.

CONCLUSIONS

The results of this study demonstrate that proper analysis of transient-response experiments for Fischer–Tropsch synthesis must account for the effects of product physisorption on the catalyst and for the reentry of olefins into the chain growth process. Olefin reentry into the chain growth process is particularly rapid for ethylene, resulting in both initiation of new chains and the formation of monomeric building units, the latter formed as a result of depolymerization of ethyl groups. For the conditions studied, reentry of C_{3+} olefins is negligible for low catalyst bed residence times but can become important for olefins containing more than eight carbon atoms when the catalyst bed residence time is large. From simulations of the transient-response data, using theoretical expressions based on the reaction scheme shown in Fig. 8, rate coefficients are calculated for each of the elementary processes involved in Fischer–Tropsch synthesis.

The surface coverages by monomeric building units and alkyl species have also been determined from an analysis of the fitted transient response curves. Monomeric building units are found to occupy about 0.2 ML, whereas, growing alkyl species occupy less than 0.1 ML. These coverages are found to be in reasonable agreement with recent experimental estimates of these species.

APPENDIX

The procedure for determining the rate parameters and coverages by each of these species illustrated in Fig. 8 was as follows. The analytical expressions for F_2, F_n (n = 3–5), and F_n^{ps} (n = 6–8) were fitted to the experimentally observed transient response curves using the nonlinear regression method described in the text. The value of τ_2 obtained by fitting the data for F_2 was used to fit the data for all of the other transients. As a consequence the transient-response data for n = 3–5 was fit with only two adjustable parameters, τ_m and τ. The values of τ_m obtained from the fitting exercise were found to be independent of the value of n for n = 2–5 and, consequently, an average value of τ_m could be used.

To carry out the above procedure for n = 6–8 requires that the values of τ_n^{ps} be known. These values were obtained by estimating the value of k_{re} and then calculating the value of τ_n^{ps} from the expression

$$\frac{1}{\tau_n^{ps}} = k_{re}\left(\frac{\theta_n^{ps}}{\theta_n^{ps}}\right) + \left(\frac{Q}{WK_nRT}\right). \qquad [A1]$$

The value of K_n appearing in Eq. [A1] is calculated by the method of Zweitering and van Krevlin (31). Figure A1 shows a plot of K_n versus n for 523 K.

For n = 3–8, is it assumed that $\tau_n = \tau = (k_p\theta_m + k_t)^{-1}$ and $\alpha_n = \alpha = k_p\theta_m/(k_p\theta_m + k_t)$. Values of k_p and k_t can be determined from

$$k_p\theta_m = \alpha/\tau \qquad [A2]$$

$$k_t = (1 - \alpha)/\tau. \qquad [A3]$$

If the values of k_p and k_t obtained for each value of n and

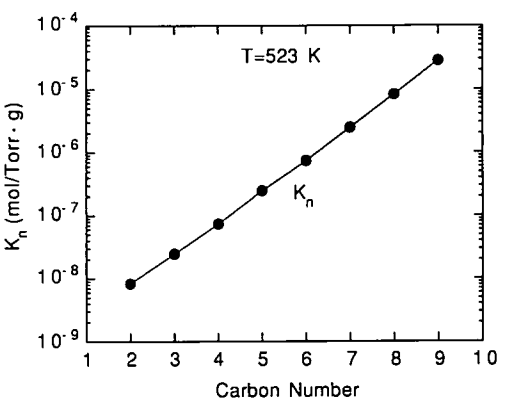

FIG. A1. K_n versus carbon number.

τ_b are not constant, the value of k_{re} is adjusted until the desired constraints on k_p and k_t are achieved.

Values of θ_m and θ_n (n = 3–8) are determined from

$$\theta_m = N_{CO}\tau_m \qquad [A4]$$

$$\theta_n = N_{C_n}/k_t. \qquad [A5]$$

The value of θ_2 is determined by a somewhat different procedure. A value of k'_{re} is chosen and the magnitude of θ_2 estimated from

$$\theta_2 = \frac{N_{C_2} + k'_{re}\theta_2^{ps}}{k_t} \qquad [A6]$$

This value of θ_2 is then substituted into Eq. [A7], to calculate τ_2:

$$\frac{1}{\tau_2} = \frac{1}{\tau} - k'_{re}\left(\frac{\theta_2^{ps}}{\theta_2}\right) + k_{dp}. \qquad [A7]$$

The values of k'_{re} and k_{dp} are not adjusted to obtain a fit to the curve of τ_2 versus τ_b. The value of θ_1 was assumed to be proportional to the value of θ_m.

Values of k_i and k_{ir} are found by fitting the values of τ_m obtained for different values of τ_b to the expression given by

$$\frac{1}{\tau_m} = \left(k_i + k_p \sum_{n=1}^{\infty} \theta_n\right) - k_{ir}\left(\frac{\theta_1}{\theta_m}\right) - k_{dp}\left(\frac{\theta_2}{\theta_m}\right). \qquad [A8]$$

As a check of the assumption that $\tau_1 = \tau_2$, the value of τ_1 is determined from

$$\frac{1}{\tau_1} = (k_t + k_p\theta_m) + k_{ir} - k_{dp}\left(\frac{\theta_2}{\theta_1}\right). \qquad [A9]$$

The values of τ_1 calculated using Eq. [A9] are similar to those determined from the fit of Eq. [20] to the experimentally observed curves of $F_2(t)$, demonstrating the internal consistency of the approach used for analysis of the transient response experiments.

ACKNOWLEDGMENT

This work was supported by the Director, Office of Basic Energy Sciences, Chemical Sciences Division, of the U.S. Department of Energy under Contract DE-AC03-76SF00098.

REFERENCES

1. Anderson, R. B., "The Fischer–Tropsch Synthesis," Academic Press, New York, 1984.
2. Biloen, P., and Sachtler, W. M. H., *Adv. Catal.* **30,** 165 (1981).
3. Bell, A. T., *Catal. Rev.-Sci. Eng.* **23,** 203 (1981).
4. Dry, M. E., *in* "Catalysis Science and Technology" (J. R. Anderson and M. Boudart, Eds.), p. 150. Springer-Verlag, Berlin, 1981.
5. Vannice, M. A., *in* "Catalysis Science and Technology" (J. R. Anderson and M. Boudart, Eds.), p. 139, Springer-Verlag, Berlin, 1982.
6. Biloen, P., Helle, J. N., and Sachtler, W. M. H., *J. Catal.* **58,** 95 (1979).
7. Ekerdt, J. G., and Bell, A. T., *J. Catal.* **58,** 170 (1979); **62,** 19 (1980).
8. Bonzel, H. P., and Krebs, H. J., *Surf. Sci.* **91,** 499, (1980).
9. Kellner, C. S., and Bell, A. T., *J. Catal.* **70,** 418 (1981).
10. Winslow, P., and Bell, A. T., *J. Catal.* **86,** 158 (1984); **91,** 142 (1985).
11. Eidus, Y., *Russ. Chem. Rev.* **5,** 388 (1967).
12. Kobori, Y., Yamasaki, H., Naito, S., Onishi, T., and Tamaru, K., *J. Chem. Soc. Faraday Trans. I* **78,** 1473 (1982).
13. Jordan, D. S., and Bell, A. T., *J. Phys. Chem.* **90,** 1139 (1989).
14. Jordan, D. S., and Bell, A. T., *J. Catal.* **107,** 338 (1987); **108,** 63 (1987).
15. Iglesia, E., Reyes, S. C., and Madon, R. A., *J. Catal.* **129,** 238 (1991).
16. Madon, R. A., Iglesia, E., and Reyes, S. C., *J. Phys. Chem.* **95,** 7795 (1991).
17. Krishna, K. R., and Bell, A. T., *Catal. Lett.* **14,** 305 (1992).
18. Iglesia, E., Ryes, S. C., Madon, R. A., and Soled, S. L., *Adv. Catal.* **39,** 221 (1993).
19. Iglesia, E., Reyes, S. C., and Soled, S. L., *in* "Computer-Aided Design of Catalysts and Reactors" (C. J. Pereira and R. W. Becker, Eds.). Dekker, New York, 1993.
20. Zhang, X., and Biloen, P., *J. Catal.* **98,** 468 (1986).
21. Mims, C. A., and McCandlish, L. E., *J. Am. Chem. Soc.* **107,** 696 (1985).
22. Mims, C. A., and McCandlish, L. E., *J. Phys. Chem.* **91,** 929 (1987).
23. Yokomizo, G. H., and Bell, A. T., *J. Catal.* **119,** 467 (1989).
24. Krishna, K. R., and Bell, A. T., *J. Catal.* **139,** 104 (1993).
25. Sano, M., Yotsui, Y., Abe, H., and Sasaki, S., *J. Biomed. Mass Spectrosc.* **3,** 1 (1976).
26. Matthews, D. E., and Hayes, J. M., *Anal. Chem.* **50,** 1465 (1978).
27. Krishna, K. R., and Bell, A. T., *J. Catal.* **130,** 597 (1991).
28. Weinberg, W. H., *in* "Dynamics of Gas–Surface Collisions" (M. N. R. Ashfold and C. T. Rettner, Eds.). Royal Society of Chemistry, Cambridge, 1991.
29. Jenson, V. G., and Jeffreys, G. B., "Mathematical Methods in Chemical Engineering," second ed. Academic Press, New York, 1977.
30. Box, G. E. P., Hunter, W. G., and Hunter, J. S., "Statistics for Experiments," Wiley, New York, 1978.
31. Gregg, S. J., and Sing, K. S. W., "Adsorption, Surface Area, and Porosity," Academic Press, New York, 1967.